Point defect engineering of high temperature piezoelectric $BiScO_3$-$PbTiO_3$ for enhanced voltage response

C. Pascual-González[+], E. Berganza, H. Amorín, A. Castro, M. Algueró*

Instituto de Ciencia de Materiales de Madrid, CSIC. Cantoblanco, 28049 Madrid, Spain

*Corresponding author: Miguel Algueró (E-mail address: malguero@icmm.csic.es)

[+] Current address: Materials Engineering and Research Institute, Sheffield Hallam University. Howard Street, Sheffield, S1 1WB, UK

ABSTRACT

$BiScO_3$-$PbTiO_3$ is the most promising system among high sensitivity piezoelectric $BiMO_3$-$PbTiO_3$ perovskite solid solutions with high Curie temperature, which are under extensive investigation for expanding the operation temperature of state of the art $Pb(Zr,Ti)O_3$ (PZT) up to 400 ºC. The viability of these alternative materials requires the development of a specific point defect engineering that allow a range of piezoelectric ceramics comparable to commercial PZTs to be obtained, optimized for the different applications. A distinctive feature of $BiMO_3$-$PbTiO_3$ systems is the simultaneous presence of both Bi^{3+} and Pb^{2+} at the A-site of the perovskite. This enables the possibility of introducing charged point defects without incorporating new chemical species, just by defining an A-site non–stoichiometry. In this work, we present a comprehensive study of the effects of Bi substitution for Pb, along with the formulation of Pb vacancies for charge compensation. Results indicate an overall lattice stiffening that yields reduced polarizability and compliance, and dominates over a limited enhancement of the ferroelectric domain wall dynamics, so as a largely enhanced voltage response is obtained. Specifically, $BiScO_3$-$PbTiO_3$ with the *A*-site non-stoichiometry is shown to be very suitable as the piezoelectric component of magnetoelectric composites for magnetic field sensing.

Keywords: Electroceramics; Perovskites; Piezoelectricity; Morphotropic Phase Boundary; Point defects

1. Introduction

The very high piezoelectric response of the $Pb(Zr,Ti)O_3$ (PZT) and $BiScO_3$-$PbTiO_3$ perovskite solid solutions at their morphotropic phase boundary (MPB) is known to result from the presence of an intermediate monoclinic phase with *Cm* space group between the ferroelectric polymorphs of rhombohedral *R*3*m* and tetragonal *P*4*mm* symmetry, which provides a structural bridge between them [1-3], and the occurrence of lattice transverse softening at the monoclinic-tetragonal boundary [4,5]. This results in very high transverse polarizability and thus, shear piezoelectricity that are ultimately responsible of the high effective piezoelectric coefficient. However, this single crystal contribution only account for 1/3 of the total piezoelectric coefficient of PZT ceramics [6].

The additional, actually major piezoelectric response is originated from ferroelectric/ ferroelastic domain wall movements [6,7]. Indeed, the tailoring of this contribution by point defect (or chemical) engineering of $Pb(Zr,Ti)O_3$ has been key to the success of this material technology, enabling the available wide family of high sensitivity piezoelectric ceramics optimized for a range of applications. It is acknowledged that the viability of alternative materials requires the development of analogous point defect engineering for the novel compounds. This is the case of the $BiMO_3$-$PbTiO_3$ systems, which have the potential of expanding the operation temperature of state of the art high sensitivity piezoelectric ceramics beyond 200 ºC and up to 400 ºC. [8-12]. Though these systems, and specifically $BiScO_3$-$PbTiO_3$ concentrate an increasing attention, this mainly focuses on optimizing processing [13-15], and little work has been carried out on property engineering though the controlled introduction of point defects.

Roughly speaking there are two main families of $Pb(Zr,Ti)O_3$ based materials referred to as hard and soft PZTs. The former group is characterized by reduced domain wall activity and thus,

small dielectric and mechanical losses. Mn and Fe co-modified $BiScO_3$-$PbTiO_3$ has been recently shown to be a hard material with a Curie temperature of 492 ºC and a d_{33} coefficient of 235 pC N^{-1}, while presenting very low electrical and mechanical losses, thus suitable for high power applications [16].Hardening has also been reported to result from Cr_2O_3 doping [14].

On the contrary, soft PZT is characterized by an enhanced domain wall activity and thus, the largest piezoelectric coefficients but also significant dielectric and mechanical losses. This is achieved by substitution of either trivalent species, such a La^{3+} for Pb^{2+} at the A-site, or pentavalent species like Nb^{5+} for Ti/Zr^{4+} at the B-site. This is thought to introduce A-site cation vacancies for charge compensation that interact with the walls increasing their mobility, yet the actual mechanism is not well understood [17]. Soft PZTs can show piezoelectric coefficients as high as 600 pC N^{-1} and are used for non-resonant applications, like actuation, whenever hysteresis is not an issue [7,18].

There have been a number of attempts to apply similar concepts to $BiScO_3$-$PbTiO_3$ for softening with little success. The introduction of La^{3+} substituting for Pb^{2+} in the A-site was firstly investigated [19]. Charge compensation was addressed by formulation of Ti vacancies in this work. A linear decrease of the Curie temperature with the addition of La of -21 ºC $(mol\%\ La)^{-1}$ was found as the main effect, along with a significant grain size reduction. A comparison of the properties of materials with similar grain size indicated a moderate enhancement of dielectric losses and of the d_{33} piezoelectric coefficient up to 550 pC N^{-1} after La addition. These effects together with a slight decrease of coercive field suggest a limited increase of the domain wall mobility.

The introduction of Nb^{5+} substituting for Ti^{4+} in the B-site of the perovskite has also been studied [20]. Charge compensation was addressed by formulation of Pb vacancies, though an initial excess of PbO and Bi_2O_3 was also introduced, and sintering was carried out in the

presence of sacrificial powder. Main effects were a continuous decrease of Curie temperature and tetragonal distortion, but little changes in the electrical and electromechanical properties. Additionally, grain growth was inhibited. Unfortunately results do not allow a direct comparison of the properties of ceramics with the same grain size, though a slight increase in domain wall mobility after Nb substitution is suggested by the small decrease in coercive field from 2.6 down to 2.4 kV mm^{-1}. This cannot be explained with the decrease in grain size.

Finally, the introduction of Zr^{4+} substituting for Sc^{3+} in $0.37BiScO_3$-$0.63PbTiO_3$ was later investigated [21]. Charge was not compensated by formulation this time. Although the room temperature (RT) permittivity and remnant polarization were enhanced by about 25%, dielectric losses decreased and coercive field increased. Therefore, enhancement cannot be rationalized as an increase in the domain wall mobility. Also, the linear piezoelectric coefficient was reduced.

A main issue in all these investigation was the use of weight% excesses of PbO and Bi_2O_3 into the initial mixture, and of sacrificial powder during sintering. This strongly hinders the controlled introduction of A-site vacancies for charge compensation, and can strongly affect microstructure and even phases, for one cannot assume that the volatilization/condensation kinetics is the same for the two binary oxides. Indeed, an excess of Bi_2O_3 has been tested as a liquid phase forming during sintering, and surprisingly found to cause a decrease of grain size, and an improvement of properties [22].

A distinctive feature of $BiMO_3$-$PbTiO_3$ systems is the simultaneous presence of both Bi^{3+} and Pb^{2+} at the A-site of the perovskite. This enables the possibility of introducing charged point defects without incorporating new chemical species, just by defining an A-site non–stoichiometry. It is worth noting that softening is suggested as a result of the excess of Bi_2O_3 in ref. 22. In this second paper, we report a comprehensive study of the effect of Bi substitution for Pb, along with the formulation of Pb vacancies for charge compensation, into $BiScO_3$-$PbTiO_3$. Care was taken to

tailor processing in order to obtain ceramic materials with controlled phase coexistence within the MPB region, and increasing levels of Bi substitution. This allowed the effect of point defects to be described for the two perovskite polymorphic phases.

2. Experimental

Dense, highly homogenous ceramic materials were processed from nanocrystalline powders obtained by mechanochemical activation of precursors in a high energy planetary mill. This is a powerful technique for the synthesis of nanocrystalline functional oxides, which allows most known, technologically relevant perovskite compounds to be obtained [23-28]. Specifically, perovskite single phase nanocrystalline powders of $Bi_{1-x+2y}Pb_{x-3y}Sc_{1-x}Ti_xO_3$ with $0.64 \leq x \leq 0.68$ and y=0, 0.01 and 0.025 were synthesized by mechanochemical activation of stoichiometric mixtures of analytical grade Bi_2O_3 (Aldrich, 99.9% pure), Sc_2O_3 (Aldrich, 99.9% pure), PbO (Merck, 99% pure), and TiO_2 (anatase, Cerac, 99% pure) with a Pulverisette 6 model Fritsch planetary mill. In all cases, about 10 g of the mixture of the precursor oxides was initially homogenized by hand in an agate mortar, and placed in a tungsten carbide (WC) jar of 250 ml with seven, 2 cm diameter, 63 g mass each WC balls for activation at 300 r.p.m., for 20 h. These conditions have been shown to provide perovskite single phase fully crystalline powders with nanometer-scale chemical homogeneity [29,30], and are shown here to result in the controlled incorporation of point defects into the perovskite.

Ceramic processing was carried out by conventional means. About 1 g of nanocrystalline powder was uniaxially pressed into 12 mm diameter pellets, which were then sintered in a closed Al_2O_3 crucible inside a furnace. A temperature of 1100 ºC, a soaking time of 1 h and heating/cooling rates of ± 3 ºC min^{-1} were selected. Significant PbO or Bi_2O_3 losses did not take

place under these conditions, as checked by monitoring weight changes after sintering. This is thought to be a characteristic of the perovskite nanocrystalline powders obtained by mechanosynthesis, which are fully crystallized after the mechanical treatment, and do not require any subsequent calcination step. Note that traces of PbO contamination on the crucible inner walls were not found at the sintering temperature used. Negligible losses allowed the use of initial precursor excesses or of sacrificial powder; that is, to bury the green bodies in powder during the thermal treatment, to be avoided. This highly facilitates composition and phase coexistence control, specially an issue in the current investigation. Densification values above 95% were consistently achieved.

Samples for phase and microstructural characterizations were prepared by thinning of ceramics to remove one surface (~100 μm), followed by polishing to a mirror finish. This also removes possible surface composition deviations that could have gone unnoticed. A final thermal treatment at 600 ºC for 2 h with ± 0.5 ºC min^{-1} was carried out to remove the damage introduced, and to restore the equilibrium polymorphic phase coexistence and domain configurations, which are modified by the shear stresses involved in polishing [31].

Perovskite phase stability during sintering was controlled by X-ray diffraction (XRD) with a Siemens D500 powder diffractometer and Cu K_α radiation (λ=1.5418 Å). Patterns were recorded between 20 and 50º (2θ) with 0.05º (2θ) step and 5 s counting rate. Slow scans; 0.02º (2θ) step and 10 s counting rate, were carried out between 43 and 47º (2θ) across the perovskite parent cubic phase 200 diffraction peak, for the analysis of the ferroelectric distortion and the evaluation of the phase percentages within the coexistence region.

Microstructure was studied with a FEI Nova™ NanoSEM 230 field emission gun scanning electron microscope equipped with an Oxford INCA 250 electron dispersive X-ray spectrometer for chemical analysis.

Ceramic capacitor for electrical and electromechanical characterizations were prepared by thinning discs down 0.5 mm, painting of Ag electrodes on the major faces, and their sintering at 700 ºC.

Electrical characterization involved the characterization of dielectric permittivity and ferroelectric hysteresis loops. Dependences of the dielectric permittivity and losses on temperature were measured between RT and 550 ºC with a HP4284A precision LCR meter. Measurements were dynamically carried out during a heating/cooling cycle with $\pm$1.5 ºC min^{-1} rate at several frequencies between 100 Hz and 1 MHz. RT ferroelectric hysteresis loops were recorded under voltage sine waves of increasing amplitude up to 10 kV with a 0.1 Hz frequency, obtained by the combination of a synthesizer/function generator (HP 3325B) and a high voltage amplifier (TREK model 10/40), while charge was measured with a homebuilt charge to voltage converter and software for loop acquisition and analysis.

Subsequently, the ceramic discs were poled for electromechanical characterization. A field of 4 kV mm^{-1} was applied at 100 ºC for 15 min, and maintained during cooling down to 40 ºC. These are standard conditions for the poling of $BiScO_3$-$PbTiO_3$ ceramics [8-10]. The longitudinal piezoelectric coefficient d_{33} was then measured 24 h after the poling step with a Berlincourt type meter. Also, the transverse piezoelectric coefficient d_{31} was obtained by complex analysis of piezoelectric radial resonances of the discs by an automatic iterative method described elsewhere [32]. This procedure also provides the s_{11}^E and s_{12}^E compliances and ε_{33}^σ permittivity of the poled material all in complex form and thus, all mechanical, electrical and electromechanical losses.

Finally, magnetoelectric transducers were fabricated with selected $Bi_{1-x+2y}Pb_{x-3y}Sc_{1-x}Ti_xO_3$ compositions. Three-layer structures consisting of one piezoelectric ceramic disc, glued between two Terfenol-D metal alloy pieces (ETREMA Products Inc.) by using a silver loaded epoxy

adhesive were built, and their magnetoelectric response characterized. A system comprising a combination of two Helmholtz coils, designed to independently provide a static magnetic field up to 1 kOe to magnetize the material, and an alternate magnetic field up to 10 Oe at 10 kHz to play as stimulus (Serviciencia S.L.) was used, while the magnetoelectric voltage response was monitored with a lock-in amplifier. A 3-1 geometry was chosen to obtain the transverse magnetoelectric coefficient α_{31} as a function of the bias magnetic field *H*, after normalization to the piezoelectric element thickness (0.5 mm).

3. Results and discussion

XRD patterns for $Bi_{1-x+2y}Pb_{x-3y}Sc_{1-x}Ti_xO_3$ with x=0.64 and y=0, 0.01 and 0.025 are shown in Fig. 1. No secondary phases in addition to the perovskite one are found in the ceramics with y=0 and 0.01, while an unidentified small diffraction peak appears in the sample with y=0.025, suggesting the substitution of Bi for Pb to be incomplete at this nominal level.

Patterns with improved statistics across the perovskite parent cubic phase 200 diffraction peak, along with their deconvolution by using three pseudo-Vöigt functions are given in Fig. 2. Coexistence of rhombohedral and tetragonal phases is assumed for simplicity, even though the former polymorph is known to most probably be monoclinic. This can be done because the monoclinic distortions only result in an additional broadening of the rhombohedral peaks in ceramics, when conventional powder diffraction is used. Results indicate all materials with increasing amount of Bi substitution to be within the MPB region, yet the percentage of rhombohedral phase clearly increases with y, while the tetragonal distortion decreases.

Scanning electron microscopy (SEM) images of the three materials with an increasing amount of Bi substituting for Pb are shown in Fig. 3. A homogenous microstructure with average grain sizes of 2.4, 1.2 and 1.3 μm for y=0, 0.01 and 0.025, respectively, was obtained. A distinctive decrease in grain size thus resulted. Grain growth inhibition has also been observed after La^{3+} substitution for Pb^{2+} in the A-site [19], Nb^{5+} substitution for Ti^{4+} or Zr^{4+} for Sc^{3+} in the B-site [20,21], and after addition of Bi_2O_3 excess [22], all requiring cation vacancies for charge compensation. Therefore, one can assume an effect of vacancies at grain boundaries dragging them, and thus hindering grain growth.

The preliminary characterization confirms that this first series of materials is not suited to study the effect of the A-site non-stoichiometry in properties, for concomitant phase and microstructural effects are found that complicate the discussion. In order to obtain a series of ceramic materials with comparable phase coexistence and increasing concentrations of $Bi_{Pb}^{\bullet}$ and V_{Pb}'' point defects, the initial (1-x)$BiScO_3$-x$PbTiO_3$ composition was shifted towards the tetragonal side. A new series of ceramics with x=0.65 and y=0.01; x=0.66 and y=0.01 and 0.025; and x=0.68 and y=0.025 were processed and characterized. Microstructure coarsening was also targeted, so sintering experiments at 1125 and 1150 ºC were additionally carried out.

Indeed the material with x=0.66 and y=0.01 showed phase coexistence comparable to that of the initial unmodified material (without point defect engineering, this is with x=0.64 and y=0). Its XRD pattern is shown in Fig. 4, along with that of the ceramic with x=0.64 and y=0.01. Note the slight increase of tetragonal distortion with x, consistent with previous reports for the $BiScO_3$-$PbTiO_3$ system [8]. Therefore, a material having an A-site non-stoichiometry, while still being at the core of the MPB has been chemically engineered, directly comparable to the reference material. However, only a limited microstructure coarsening was obtained by increasing sintering temperature: average grain size of 1.4 and 1.6 μm with 1125 and 1150 ºC, respectively (see also Fig. 4). This further supports the main role of Pb vacancies in grain growth by dragging the grain

boundaries. Temperatures above 1150ºC could not be used, for PbO and Bi_2O_3 volatilization started being an issue. Final slight differences in grain size, 2.4 against 1.6 μm, will be taken into account when discussing the effect of the $Bi_{Pb}^{\bullet}$ and V_{Pb}'' point defects in properties.

A material with y=0.025 and phase coexistence comparable to that of the reference material could not be obtained, as illustrated in Fig. 5. XRD patterns of ceramics with x=0.66 and 0.68 and y=0.025 did not show an increase in the percentage of the tetragonal phase as targeted, but its apparent disappearance, and the development of a new peak at a lower º2θ angle than the tetragonal 002 (labeled with **?** in the Figure). No second phase was found in the SEM images (also presented in Fig. 5). It is worth noting that this peak was also observed in a ceramic with x=0.66 and y=0.01 that have been sintered at 1150 ºC under prolonged heating, this time together with the peaks corresponding to both the tetragonal and rhombohedral polymorphs (see inset). Again, SEM did not show any trace of second phases. These observations suggest this peak to be associated with an additional perovskite phase of composition and structural parameters not far to those of the coexisting polymorphs, but pseudocubic. This phase develops when $Bi_{Pb}^{\bullet}$ and V_{Pb}'' point defects above a certain level are formulated into the tetragonal phase, or below this threshold as a result of a prolonged heating. It is thus hypothesized that this phase might be a grain boundary one caused by the accumulation of point defects, which are segregated from the coexisting tetragonal component, accepting its low tolerance to the incorporation of the specific defects. Though the material with y=0.025 is not suitable to study the effect of the A-site non-stoichiometry, its properties will be presented along with those of y=0.01 for comparison, and further discussion of the proposed mechanisms.

The temperature dependence of the dielectric permittivity for the different $Bi_{1-x+2y}Pb_{x-3y}Sc_{1-x}\ Ti_xO_3$ materials are shown in Fig. 6, while ferroelectric hysteresis loops are given in Fig. 7. Curves corresponding to the initial series of materials with x=0.64 and an increasing amount of Bi substitution are given in Fig. 6(a) and 7(a). Note firstly in the former figure

the continuous decrease of the Curie temperature with y. The dielectric anomaly associated with the ferroelectric transition is observed at a temperature of 450, 395 and 375 ºC for y=0, 0.01 and 0.025, respectively. A distinctive increase of the RT permittivity and losses of the unpoled ceramics with increasing Bi substitution is also found. Specific values are given in Table 1, along with the T_Cs.

This simultaneous increase of permittivity and losses might be interpreted as the targeted enhancement of the domain wall mobility. Indeed ferroelectric hysteresis loops show a distinctive decrease of the coercive field, from 2.5 down to 2.0 kV mm^{-1}, when a Bi substitution of y=0.01 is introduced, at the same time that the remnant polarization increases from 40 up to 44 $\mu C\ cm^{-2}$. Furthermore, this takes place in spite of the decrease of grain size that is known to increase the coercive field [33]. However, this apparent softening might also be caused by the observed shift of the phase coexistence towards the rhombohedral polymorph, for its coercive field is lower than that of the tetragonal phase.

This possibility can be assessed by comparing the properties of the unmodified material with those of the ceramic with x=0.66 and y=0.01, which show comparable phase coexistence, and is thus also at the core of the MPB. Results for the series of ceramics with increasing values of x and y=0.01 are presented in Fig. 6(b) and 7(b). Note in the former figure the continuous increase of the Curie temperature with x. The dielectric anomaly associated with the ferroelectric transition is observed at a temperature of 395, 407 and 415 ºC for x=0.64, 0.65 and 0.66, respectively. This is the expected behavior when one moves towards the tetragonal side along the $BiScO_3$-$PbTiO_3$ system [8]. No systematic trends of the RT permittivity and losses of the unpoled ceramics were found, while values remain higher than those of the reference material. Specific values are also given in Table 1, along with T_C ones.

Ferroelectric hysteresis loops do change. Coercive field increases with x, such as the ceramic material with x=0.66 and y=0.01 has the same coercive field than that of the unmodified material (x=0.64, y=0), but a slightly smaller remnant polarization of 35 $\mu C\ cm^{-2}$. These are the two materials with analogous phase coexistence, so they can be directly compared to evaluate the targeted enhancement of the domain wall mobility after the introduction of the point defects. A limited softening can only be concluded, for coercive field does not decrease, even though the RT dielectric permittivity and losses do increase.

Results for the series of ceramics with increasing x and y=0.025 are presented in Fig. 6(c) and 7(c). Note in the former figure the continuous increase of the Curie temperature with x. The dielectric anomaly associated with the ferroelectric transition is observed at a temperature of 375, 388 and 408 ºC for x=0.64, 0.66 and 0.68, respectively. As already pointed out, this is the expected behavior when one moves towards the tetragonal side along the $BiScO_3$-$PbTiO_3$ system, but it is not consistent with the structural characterization that indicated the disappearance of the tetragonal polymorph, and development of a new pseudocubic perovskite phase. This strongly supports the hypothesis of it being a grain boundary phase formed by accumulation of point defects, segregated from the tetragonal polymorph that cannot accommodate them. Indeed the observed systematic decrease of the RT permittivity and losses with x for y=0.025 supports this scenario, as well as the increase of the coercive field up to 3.0 $kV\ mm^{-1}$. General features of the materials with y=0.025, such as the strong depletion of the dielectric anomaly at the ferroelectric transition, and the comparatively low remnant polarization values around 30 $\mu C\ cm^{-2}$ also indicate it.

Charge longitudinal and transverse piezoelectric coefficients after poling are given in Table 1. Further discussion will be restricted to materials with x=0.64 and an increasing amount of Bi substituting for Pb, and to that one tailored to remain at the core of the MPB after introducing the A-site non-stoichiometry: x=0.66 and y=0.01. Ceramics with x=0.64 show a continuous decrease

of the d_{33} piezoelectric coefficient with y, from 440 down to 412 and 312 pC N^{-1} for y=0, 0.01 and 0.025, respectively. This does not agree with the observed increase in permittivity of the unpoled ceramics with y, but it is consistent with the already discussed shift of phase coexistence towards the rhombohedral side. However, when x was increased while maintaining y=0.01 to correct the latter phase shift, d_{33} did not increase but continuously decreased, from 412, down to 404 and 366 pC N^{-1} for x=0.64, 0.65 and 0.66, respectively. Same trends were obtained for the d_{31} piezoelectric coefficient. We will come back to these apparent contradictions later on.

The complex analysis of piezoelectric radial resonances that provides the d_{31} piezoelectric coefficient, also renders the s_{11}^E and s_{12}^E compliances and ε_{33}^σ permittivity of the poled ceramics, all in complex form and thus, the mechanical, electrical and electromechanical losses. A first result worth commenting on is the very large enhancement of permittivity experienced by the materials at the core of the MPB after poling. The permittivity of the unmodified high sensitivity $BiScO_3$-$PbTiO_3$ increased from 835 up to 1486, while dielectric losses did not change. A comparably large increase; from 2400 up to 3900 has been reported for coarse grained (10 μm) soft PZT upon poling [34]. Reasons behind this are not clear, but cannot be associated with an enhancement of the domain wall contribution, for wall density must be strongly reduced upon poling. An alternative mechanism might be the anisotropy in single crystal permittivity; this is ε_{33} being significantly higher than ε_{11}, but experimental permittivity values for poled ceramics do not indicate this to be the case [35]. Changes in the stress state or/and in the percentage of phases in coexistence at the MPB upon poling could be responsible for the permittivity increase that also takes place in the material including $Bi_{Pb}^{\bullet}$ and V_{Pb}'' point defects (x=0.66 and y=0.01). Indeed materials with initial phase coexistence shifted towards the rhombohedral side; those with x=0.64 and y=0.01 and 0.025 do not show a comparable increase.

A second result worth stressing out is the distinctive decrease of the elastic compliances of the poled ceramics after the introduction of the A-site non-stoichiometry. This takes place for the series of materials with x=0.64 and increasing y, and also for the material tailored to remain at the core of the MPB, while incorporating the $Bi_{Pb}^{\bullet}$ and V_{Pb}'' point defects. This latter material does not only show smaller piezoelectric coefficients and elastic compliances than the unmodified $BiScO_3$-$PbTiO_3$, but also a smaller permittivity after poling, and decreased dielectric, mechanical and electromechanical losses.

A thorough analysis of the effects of the introduction of the point defects, and of the functionality of the chemically engineered materials can be done now. Though the electrical properties of the unpoled ceramics suggested the introduced A-site non-stoichiometry to cause a limited enhancement of the domain wall mobility as targeted, the response of the poled materials does not reflect this enhancement, most probably due to the strongly decreased wall density (and the dominance of single crystal effects in this state). Therefore, a soft $BiScO_3$-$PbTiO_3$ was not obtained by the substitution of Bi for Pb, and introduction of additional Pb vacancies for charge compensation. These results are qualitatively similar to those obtained with different heterovalent substitutions in either the A- or the B-site [19-21]. Overall, this seems to indicate the existence of significant differences between $BiScO_3$-$PbTiO_3$ and $Pb(Zr,Ti)O_3$ relating to their ability of incorporating cationic vacancies into the perovskite.

Indeed, results here reported clearly suggest the tetragonal polymorph not to incorporate the actual point defects, which are thus segregated out to the grain boundaries. This results in decreased remnant polarization, permittivity and thus, piezoelectric coefficients of materials at the core of the MPB. This effect does not seem to take place in the case of the rhombohedral polymorph that can apparently accommodate significant levels of $Bi_{Pb}^{\bullet}$ and V_{Pb}'' point defects. Actually, the properties of the materials incorporating the A-site non-stoichiometry and with phase coexistence shifted towards the rhombohedral side are remarkable and deserve discussion.

Most interesting properties are obtained for the material with x=0.64 and y=0.01 that shows an enhanced remnant polarization and decreased coercive field, which result in piezoelectric coefficients close to those of the unmodified high-sensitivity composition, but a significantly reduced dielectric permittivity (see Table 1). As a result, its voltage piezoelectric coefficient is much higher than that of the latter material. Specifically, the g_{33} coefficient increased from 3.3×10^{-2} to 4.8×10^{-2} V m N^{-1} after the incorporation of the A-site-non stoichiometry. This value is also higher than that of hard $BiScO_3$-$PbTiO_3$ reported in ref. 16: 3.3×10^{-2} V m N^{-1}. Note that this enhancement is basically a consequence of the reduced permittivity of the poled material, and it is not caused by a decrease of the domain wall contribution, but of the single crystal one, either as a consequence of the modification of the phase coexistence or a direct effect of the presence of the point defects in polarizability.

Moreover, the material has also a strongly decreased elastic compliance (one can assume then that the incorporation of the point defects causes an overall increase of the lattice rigidity with a direct effect on polarizability and deformability). One of the most topical new application of high-sensitivity piezoelectrics is as component of magnetoelectric composites, in which they are combined with magnetostrictive materials to provide magnetoelectricity as a product property [36-38]. Magnetoelectric transducers are being considered for a range of technologies like high-sensitivity magnetic field sensors with RT operation [39]. It has been shown that the voltage magnetoelectric coefficient of the simplest two-layer piezoelectric-magnetostrictive structure is given by [40]:

$$\alpha_{E,31} = \frac{\partial E_3}{\partial H_1} = \frac{-2d_{31}^p q_{11}^m v_m}{\left(s_{11}^m + s_{12}^m\right)\varepsilon_{33}^p v_p + \left(s_{11}^p + s_{12}^p\right)\varepsilon_{33}^p v_m - 2\left(d_{31}^p\right)^2 v_m} \quad (1)$$

where *d* and *q* are the piezoelectric and piezomagnetic coefficients of the respective phases of volume *v*, *s* are the elastic compliances, and ε the permittivity, while superindex *p* and *m* refer to the piezoelectric and magnetic component, respectively. Note that the voltage response not only increases with the reciprocal permittivity, but also with the reciprocal compliances. Therefore, the chemically engineered $BiScO_3$-$PbTiO_3$ should be especially suitable for this application.

This is demonstrated in Fig. 8, where the magnetoelectric voltage coefficient of three-layer structures fabricated with Terfenol-D and either the $BiScO_3$-$PbTiO_3$ material incorporating the A-site non-stoichiometry, or the unmodified high-sensitivity material, are compared. Indeed, the magnetoelectric coefficient is increased from about 0.2 up to more than 1 V cm^{-1} Oe^{-1} by using the piezoelectric ceramic that includes the point defect engineering.

4. Summary and conclusions

We have investigated, by using high-quality ceramic materials processed from chemically homogenous nanocrystalline powders obtained by mechanosynthesis, the effects of the introduction of increasing levels of Bi substituting for Pb, along with the necessary Pb vacancies for charge compensation, in high-sensitivity $BiScO_3$-$PbTiO_3$. Results on materials with controlled microstructure and phase coexistence across the MPB region indicate a very limited incorporation of the $Bi_{Pb}^{\bullet}$ and V_{Pb}'' point defects into the tetragonal polymorph, which are segregated out to grain boundaries during sintering. Defects do seem to incorporate into the rhombohedral phase causing changes at both the lattice and domain wall level. A distinctive enhancement of the domain wall mobility is observed, yet not to a degree high enough to dominate the response in the poled state. This is controlled by the lattice contribution, which shows a significantly reduced dielectric permittivity and elastic compliance, while maintaining high piezoelectric coefficients.

Overall, $BiScO_3$-$PbTiO_3$ with the A-site non-stoichiometry and tailored phase coexistence is an enhanced voltage response material with a Curie temperature about 400 ºC, and a g_{33} coefficient of $4.8x10^{-2}$ V m N^{-1}, higher than that previously reported for hard materials. Its use as piezoelectric component in magnetoelectric composites for magnetic sensing has been assessed. A magnetoelectric voltage response significantly higher than that of unmodified $BiScO_3$-$PbTiO_3$ is demonstrated. This is a new step towards the development of a specific point defect engineering for BMO_3-$PbTiO_3$ systems comparable to that of PZT.

Acknowledgements

Funded by Spanish MINECO through the MAT2014-58816-R and MAT2011-23709 projects. Technical supports by Ms. I. Martínez and Ms. M. M. Antón are also acknowledged.

References

[1] B. Noheda, J.A. Gonzalo, L.E. Cross, R. Guo, S.E. Park, D. Cox, G. Shirane, Tetragonal-to-monoclinic phase transition in a ferroelectric perovskite: The structure of $PbZr_{0.52}Ti_{0.48}O_3$, Phys. Rev. B 61 (2000) 8687-8695.

[2] T. Hungría, F. Houdellier, M. Alguero, A. Castro, Monoclinic symmetry of twin-free nanocrystals in the $BiScO_3$-$PbTiO_3$ solid solution as revealed by aberration-corrected TEM, Phys. Rev. B 81 (2010) art. nº 100102(R).

[3] K.V. Lalitha, A.K. Kalyani, R. Ranjan, Analogous stress and electric field driven structural transformation and decrease in polarization coherence on poling around the morphotropic phase boundary in $BiScO_3$-$PbTiO_3$, Phys. Rev. B 90 (2014) art. nº 224107.

[4] D. Damjanovic, Comments on origins of enhanced piezoelectric properties in ferroelectrics, IEEE Trans. Ultrason. Ferroel. Freq. Control 56 (2009) 1574-1585.

[5] K. Datta, A. Richter, M. Gobbels, D.A. Keen, R. B. Neder, Direct mapping of microscopic polarization in ferroelectric $xBiScO_3$-$(1 - x)PbTiO_3$ throughout its morphotropic phase boundary, Phys. Rev. B 93 (2016) art. nº 064102.

[6] Q.M. Zhang, H. Wang, N. Kim, L.E. Cross, Direct evaluation of domain-wall and intrinsic contributions to the dielectric and piezoelectric response and their temperature dependence on lead zirconate-titanate ceramics, J. Appl. Phys. 75 (1994) 454-459.

[7] D. Damjanovic, Ferroelectric, dielectric and piezoelectric properties of ferroelectric thin films and ceramics, Rep. Prog. Phys. 61 (1998) 1267-1324.

[8] R.E. Eitel, S.J. Zhang, T.R. Shrout, C.A. Randall, I. Levin, Phase diagram of the perovskite system $(1-x)BiScO_3$-$xPbTiO_3$, J. Appl. Phys. 96 (2004) 2828-2831.

[9] T. Zou, X. Wang, H. Wang, C. Zhong, L. Li, I.W. Chen, Bulk dense fine-grain $(1-x)BiScO_3$–$xPbTiO_3$ ceramics with high piezoelectric coefficient, Appl. Phys. Lett. 93 (2008) art. nº 192913.

[10] M. Alguero, P. Ramos, R. Jiménez, H. Amorín, E. Vila, A. Castro, High temperature piezoelectric $BiScO_3$-$PbTiO_3$ synthesized by mechanochemical methods, Acta Mater. 60 (2012) 1174-1183.

[11] J. Chen, Z. Chen, X. Li, S. Dong, A high-temperature piezoelectric linear actuator operating in two orthogonal first bending modes, Appl. Phys. Lett. 102 (2013) art. nº 052902.

[12] J.F. Wu, Y. Yu, X.T. Li, X.Y. Gao, S.X. Dong, Investigation on resonant vibration performances of Fe-doped $BiScO_3$-$PbTiO_3$ ceramics in high-temperature environment, J. Am. Ceram. Soc. 98 (2015) 3145-3152.

[13] E.D. Politova, G.M. Kaleva, A.V. Mosunov, A.H. Segalla, A.E. Dosovitskiy, A.L. Mikhlin, Processing, phase transitions, and dielectric properties of BSPT ceramics, J. Adv. Dielec. 3 (2013) art. nº 1350024

[14] A.G. Segalla, S.S. Nersesov, G.M. Kaleva, E.D. Politova, Ways of improving functional parameters of high-temperature ferroelectric/piezoelectric ceramics based on $BiScO_3$–$PbTiO_3$solid solutions, Inorg. Mater. 50 (2014) 606-611.

[15] P. Long, G. Zhang, Z. Yi, Structure and electrical behaviors of $0.36BiScO_3$–$0.64PbTiO_3$ ceramics with overdosing Bi and Pb starting materials, Mater. Res. Bull. 66 (2015) 213-218.

[16] J. Chen, G. Jin, c.M. Wang, J. Cheng, Reduced dielectric loss and astrain hysteresis in Fe and Mn comodifed high-temperature on $BiScO_3$–$PbTiO_3$ ceramics, J. Am. Ceram. Soc. 97 (2014) 3890-3896.

[17] M.I. Morozov, D. Damjanovic, Charge migration in $Pb(Zr,Ti)O_3$ ceramics and its relation to ageing, hardening, and softening, J. Appl. Phys. 107 (2010) art. nº 034106.

[18] K. Uchino, Materials issues in design and performance of piezoelectric actuators: An overview, Acta Mater. 46 (1998) 3745-3753.

[19] R.E. Eitel, T.R. Shrout, C.A. Randall, Tailoring properties and performance of (1-x)$BiScO_3$-x$PbTiO_3$ based piezoceramics by lanthanum substitution, Jpn. J. Appl. Phys. 43 (2004) 8146-8150.

[20] S. Chen, X. Dong, H. Yang, R. Liang, C. Mao, Effects of niobium doping on the microstructure and electrical properties of $0.36BiScO_3$-$0.64PbTiO_3$ ceramics, J. Am. Ceram. Soc. 90 (2007) 477-482.

[21] A. Sehirlioglu, A. Sayir, F. Dynys, Doping of $BiScO_3$-$PbTiO_3$ ceramics for enhanced properties, J. Am. Ceram. Soc. 93 (2010) 1718-1724.

[22] A. Sehirlioglu, A. Sayir, F. Dynys, High temperature properties of $BiScO_3$-$PbTiO_3$ piezoelectric ceramics, J. Appl. Phys. 106 (2009) art. nº 014102.

[23] S.E. Lee, J.M. Xue, D.M. Wan, J. Wang, Effects of mechanical activation on the sintering and dielectric properties of oxide-derived PZT, Acta Mater. 47 (1999) 2633-2639.

[24] J. Wang, D.M. Wan, J.M. Xue, W.B. Ng, Mechanochemical synthesis of 0.9 $Pb(Mg_{1/3}Nb_{2/3})O_3$-$0.1PbTiO_3$ from mixed oxides, Adv. Mater. 11 (1999) 210-213.

[25] J.M. Xue, J. Wang, D.M. Wan, Nanosized barium titanate powder by mechanical activation, J. Am. Ceram. Soc. 83 (2000) 232-234.

[26] T. Hungría, M. Alguero, A.B. Hungria, A. Castro, Dense, fine-grained $Ba_{1-x}Sr_xTiO_3$ ceramics prepared by the combination of mechanosynthesized nanopowders and spark plasma sintering, Chem. Mater. 17 (2005) 6205-6212.

[27] T. Hungría, M. Algueró, A. Castro, Synthesis of nanosized (1-x)$NaNbO_3$-x$SrTiO_3$ solid solution by mechanochemical activation, processing of ceramics, and phase transitions, Chem. Mater. 18 (2006) 5370-5376.

[28] H. Ursic, A. Bencan, G. Drazic, G. Esteves, J.L. Jones, T.M. Usher, T. Rojac, S. Drnovsek, M. Deluca, J. Jouin, V. Bobnar, G. Trefalt, J. Holc, B. Malic, Unusual structural-disorder stability of mechanochemically derived-$Pb(Sc_{0.5}Nb_{0.5})O_3$, J. Mater. Chem. C 3 (2015) 10309-10315.

[29] M. Alguero, J. Ricote, T. Hungria, A. Castro, High-sensitivity piezoelectric, low-tolerance-factor perovskites by mechanosynthesis, Chem. Mater. 19 (2007) 4982-4990.

[30] H. Amorin, T. Hungria, A.R. Landa-Canovas, M. Torres, M. Dolle, M. Alguero, A. Castro, Nanopowders of ferroic oxides for magnetoelectric composites, J. Nanopart. Res. 13 (2011) 4189-4200.

[31] M.F. Wong, K. Zeng, Mechanical polishing effects toward surface domain evolution in $Pb(Zn_{1/3}Nb_{2/3})O_3$-$PbTiO_3$ single crystals, J. Am. Ceram. Soc. 94 (2011) 1079-1086.

[32] C. Alemany, A.M. Gonzalez, L. Pardo, B. Jimenez, F. Carmona, J. Mendiola, Automatic-determination of complex constants of piezoelectric lossy materials in the radial mode, J. Phys. D: Appl. Phys. 28 (1995) 945-956.

[33] H. Amorin, R. Jimenez, M. Deluca, J. Ricote, T. Hungria, A. Castro, M. Alguero, Nanostructuring effects in piezoelectric $BiScO_3$-$PbTiO_3$ ceramics, J. Am. Ceram. Soc. 97 (2014) 2802-2809.

[34] T.M. Kamel, G. de With, Grain size effect on the poling of soft $Pb(Zr,Ti)O_3$ ferroelectric ceramics, J. Eur. Ceram. Soc. 28 (2008) 851-861.

[35] S.J. Zhang, E.F. Alberta, R.E. Eitel, C.A. Randall, T.R. Shrout, Elastic, piezoelectric, and dielectric characterization of modified $BiScO_3$-$PbTiO_3$ ceramics, IEEE Trans. Ultrason. Ferroelectr. Freq. Control 52 (2005) 2131-2139.

[36] C.W. Nan, M.I. Bichurin, S. Dong, D. Viehland, G. Srinivasan, Multiferroic magnetoelectric composites: Historical perspective, status, and future directions, J. Appl. Phys. 103 (2008) art. nº 031101.

[37] H. Amorin, M. Alguero, R. Del Campo, E. Vila, P. Ramos, M. Dolle, Y. Romaguera-Barcelay, J. Perez-De la Cruz, A. Castro, High-sensitivity piezoelectric perovskites for magnetoelectric composites, Sci. Technol. Adv. Mater. 18 (2015) art. nº 016001.

[38] Y. Song, D.A. Pan, L.R. Xu, B. Liu, A.A. Volinsky, S.G. Zhang, Enhanced magnetoelectric efficiency of the $Tb_{1-x}Dy_xFe_{2-y}$/Pb(Zr,Ti)O_3 cylinder multi-electrode composites, Mater. Des. 90 (2016) 753-756.

[39] Y. Wang, D. Gray, D. Berry, J. Gao, M. Li, J. Li, D. Viehland, An extremely low equivalent magnetic noise magnetoelectric sensor, Adv. Mater. 23 (2011) 4111-4114.

[40] G. Srinivasan, E.T. RasmussenT, J. Gallegos, R. Srinivasan, Magnetoelectric bilayer and multilayer structures of magnetostrictive and piezoelectric oxides, Phys. Rev. B 64 (2001) art. nº 214408.

Table 1 Curie temperatures and material coefficients for the $Bi_{1-x+2y}Pb_{x-3y}Sc_{1-x}Ti_xO_3$ ceramics with x=0.64, 0.65, 0.66, 0.68 and y=0, 0.01, 0.025.

		$\varepsilon_{33}^{\sigma}$ ($x\varepsilon_o$) Unpoled	Tan δ Unpoled	T_C (ºC)	d_{33} (pC N^{-1})	d_{31} (pC N^{-1})	$\varepsilon_{33}^{\sigma}$ ($x\varepsilon_o$) Poled	s_{11}^E ($x10^{-12}$ m^2 N^{-1})	s_{12}^E ($x10^{-12}$ m^2 N^{-1})
y=0	x=0.64	835	0.095	450	440	-144+15i	1486-143i	13.8-0.7i	-3.6+0.2i
y=0.01	x=0.64	920	0.105	395	412	-115+10i	966-85i	11.7-0.5i	-2.7+0.1i
	x=0.65	890	0.102	407	404				
	x=0.66	1015	0.100	415	366	-105+10i	1368-107i	11.6-0.4i	-3.4+0.1i
y=0.025	x=0.64	1045	0.127	375	312	-70+8i	1012-113i	9.9-0.3i	-2.4+0.1i
	x=0.66	970	0.117	388	320				
	x=0.68	955	0.101	408	274				

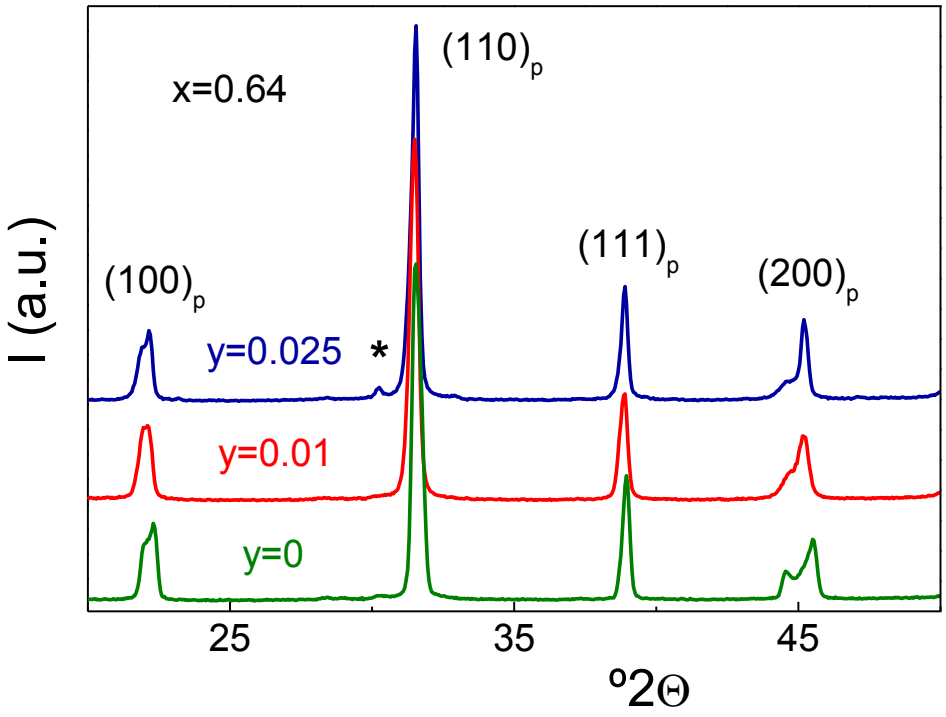

Fig. 1. XRD patterns of $Bi_{1-x+2y}Pb_{x-3y}Sc_{1-x}Ti_xO_3$ ceramics with x=0.64 and y=0, 0.01 and 0.025, showing the absence of second phases other than perovskite for y=0 and 0.01.

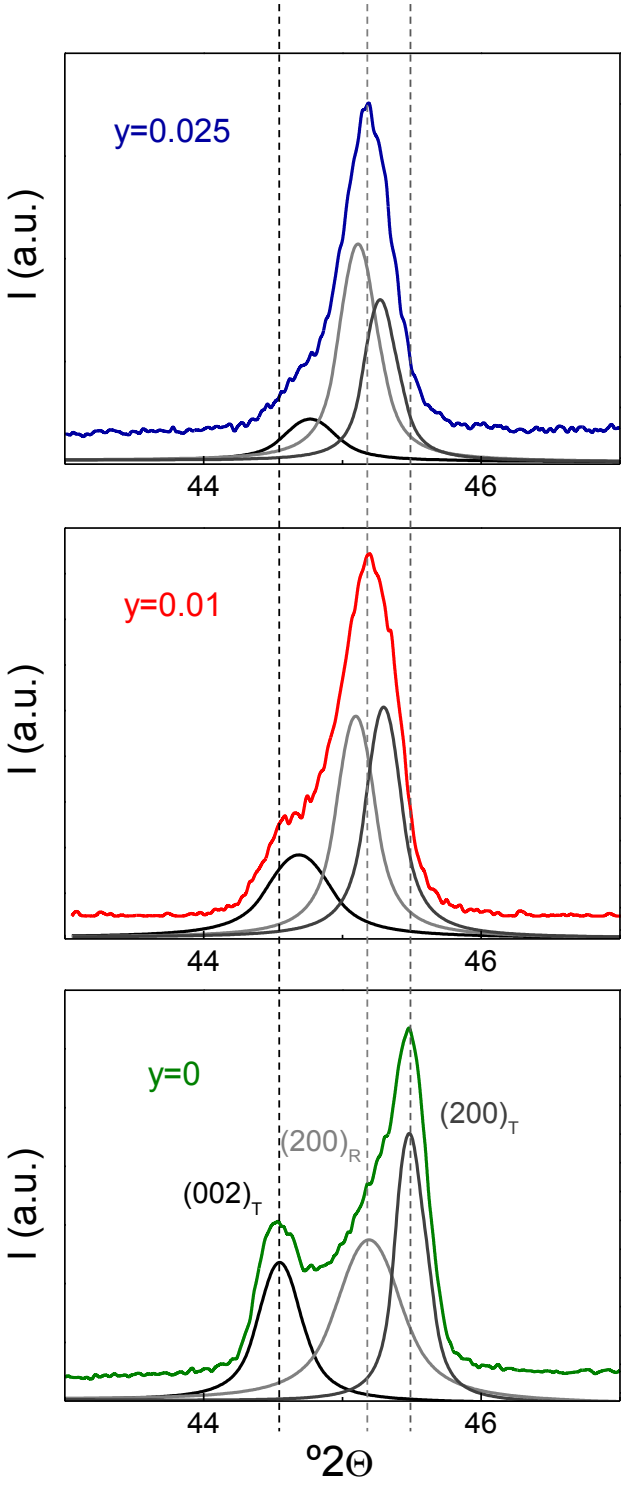

Fig. 2. XRD patterns with improved statistics across the perovskite parent cubic phase 200 diffraction peak of $Bi_{1-x+2y}Pb_{x-3y}Sc_{1-x}Ti_xO_3$ ceramics with x=0.64 and y=0, 0.01 and 0.025, showing polymorphic phase coexistence and thus, location of materials at the MPB. T and R in Miller indices stand for the tetragonal and rhombohedral symmetries, respectively.

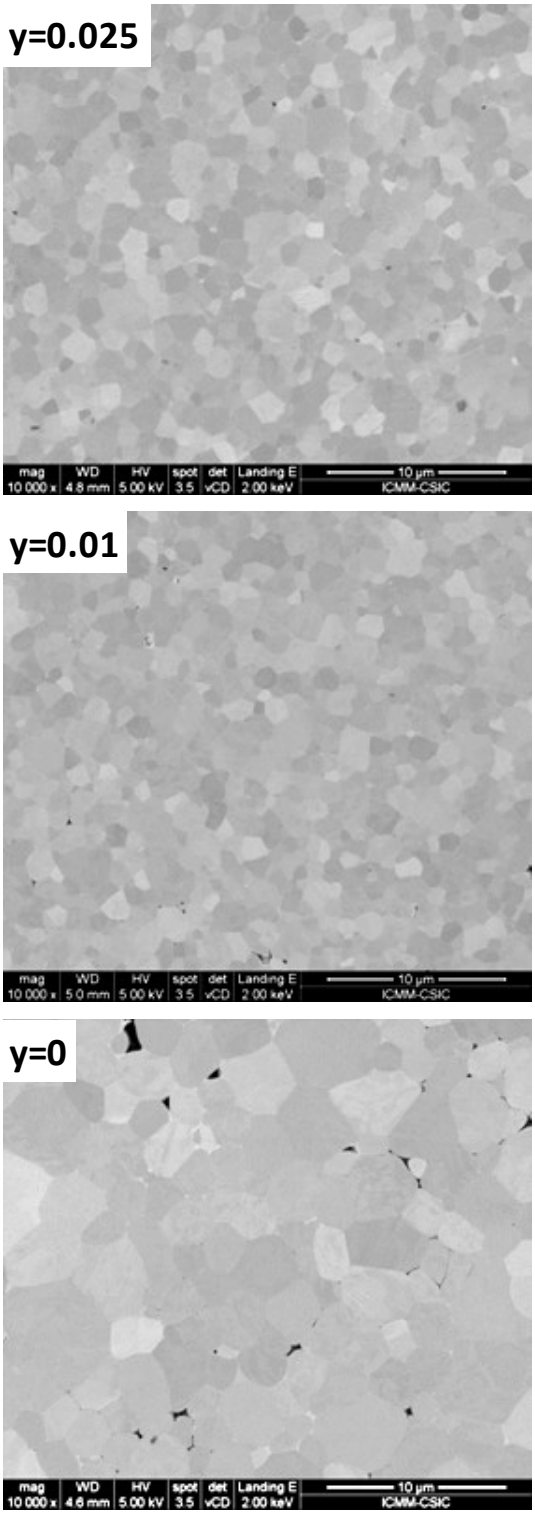

Fig. 3. SEM images of $Bi_{1-x+2y}Pb_{x-3y}Sc_{1-x}Ti_xO_3$ ceramics with x=0.64 and y=0, 0.01 and 0.025, showing dense and homogenous fine-grained microstructures.

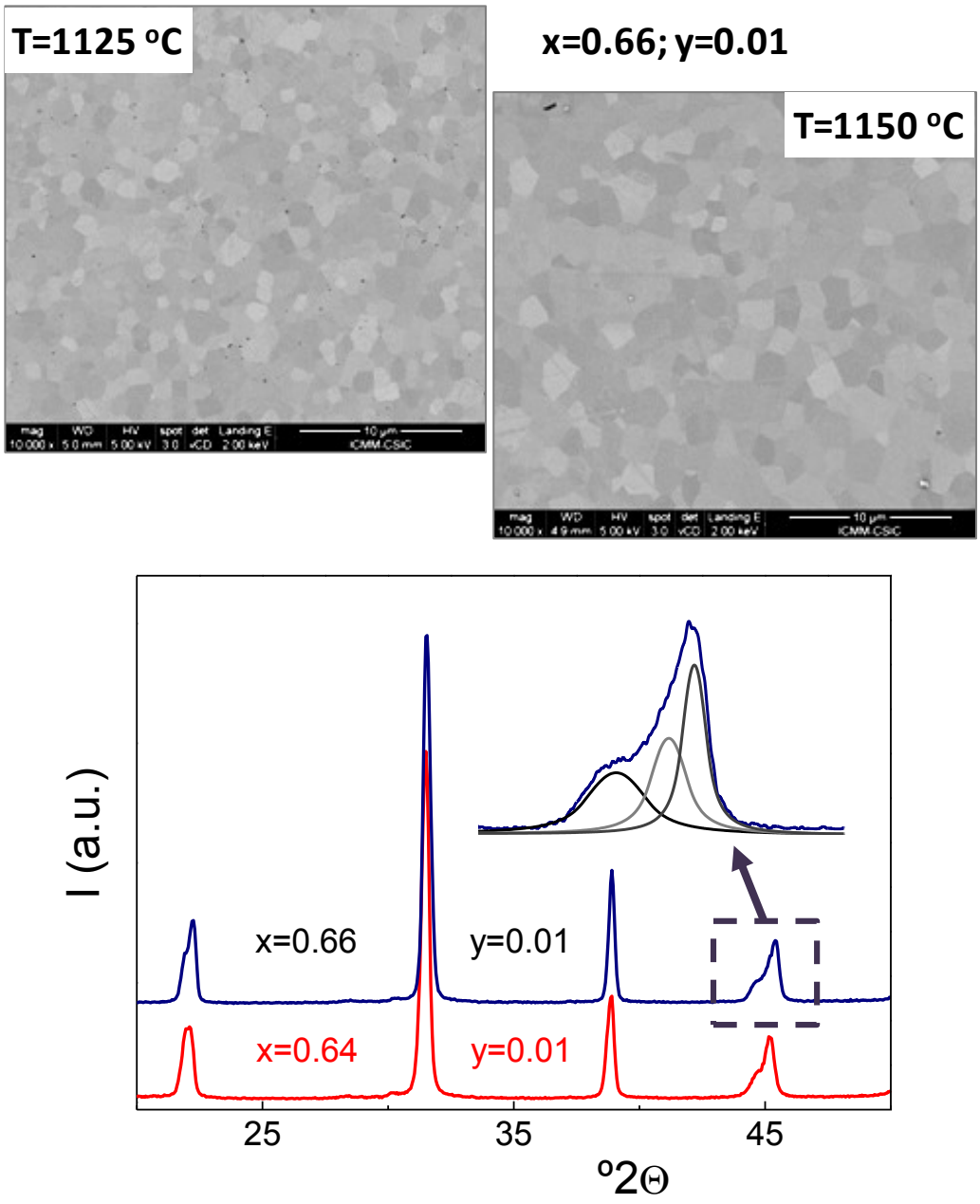

Fig. 4. SEM images of $Bi_{1-x+2y}Pb_{x-3y}Sc_{1-x}Ti_xO_3$ ceramics with x=0.66 and y=0.01, showing limited microstructure coarsening by increasing sintering temperature up to 1125 and 1150 ºC, and XRD pattern for the sample with x=0.66 and y=0.01 indicating phase coexistence comparable to that of the unmodified material; this is, with x=0.64 and y=0.

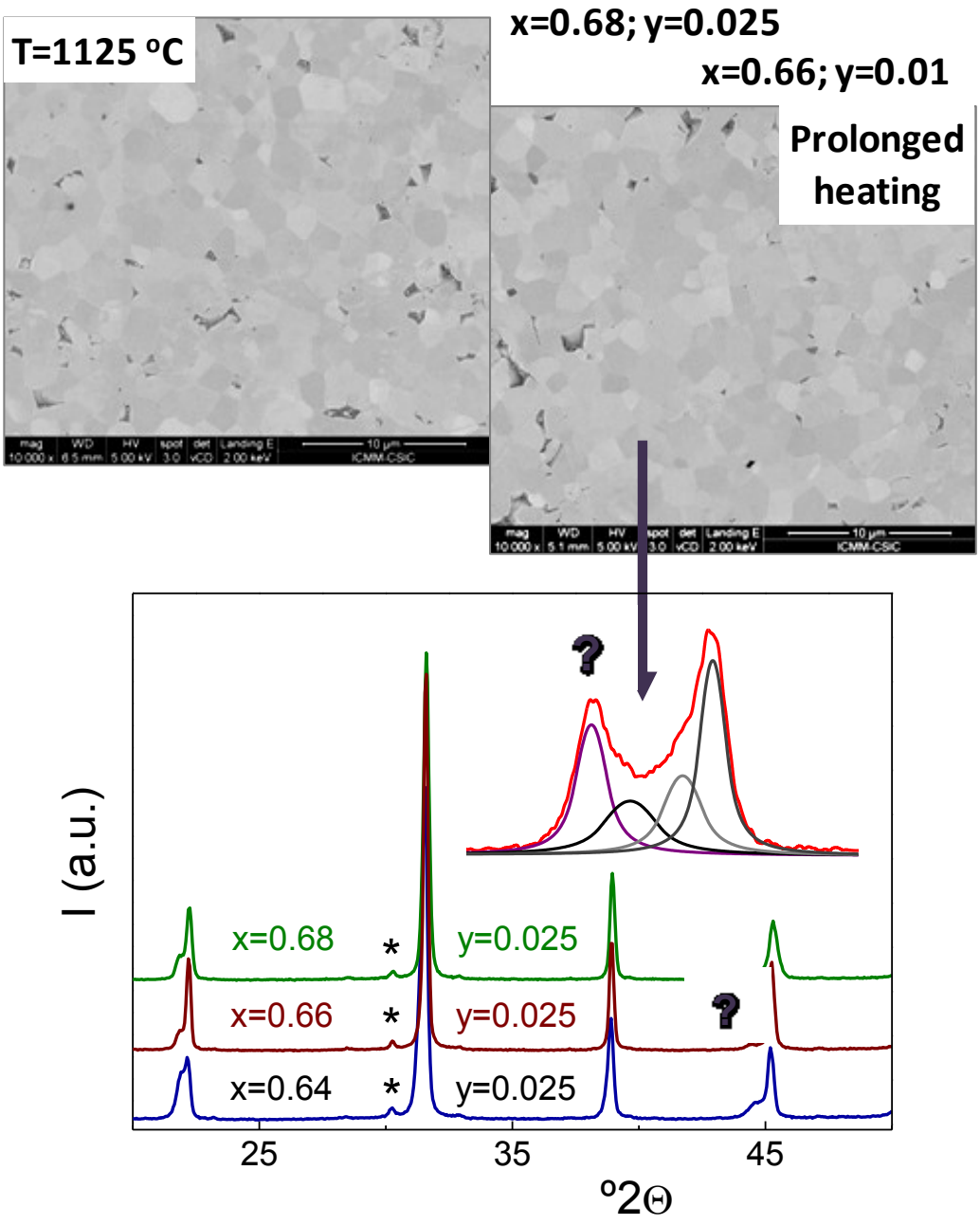

Fig. 5. SEM image of a $Bi_{1-x+2y}Pb_{x-3y}Sc_{1-x}Ti_xO_3$ ceramic with x=0.68 and y=0.025, and that for a sample with x=0.66 and y=0.01 that has undergone prolonged sintering, both with no traces of second phases; and XRD patterns of the ceramics with x=0.66 and 0.68 and y=0.025 which did not show an increase in the percentage of the tetragonal phase as targeted. The new peak at a lower º2θ angle than the tetragonal 002 (labeled with **?**) indicates an additional pseudocubic phase.

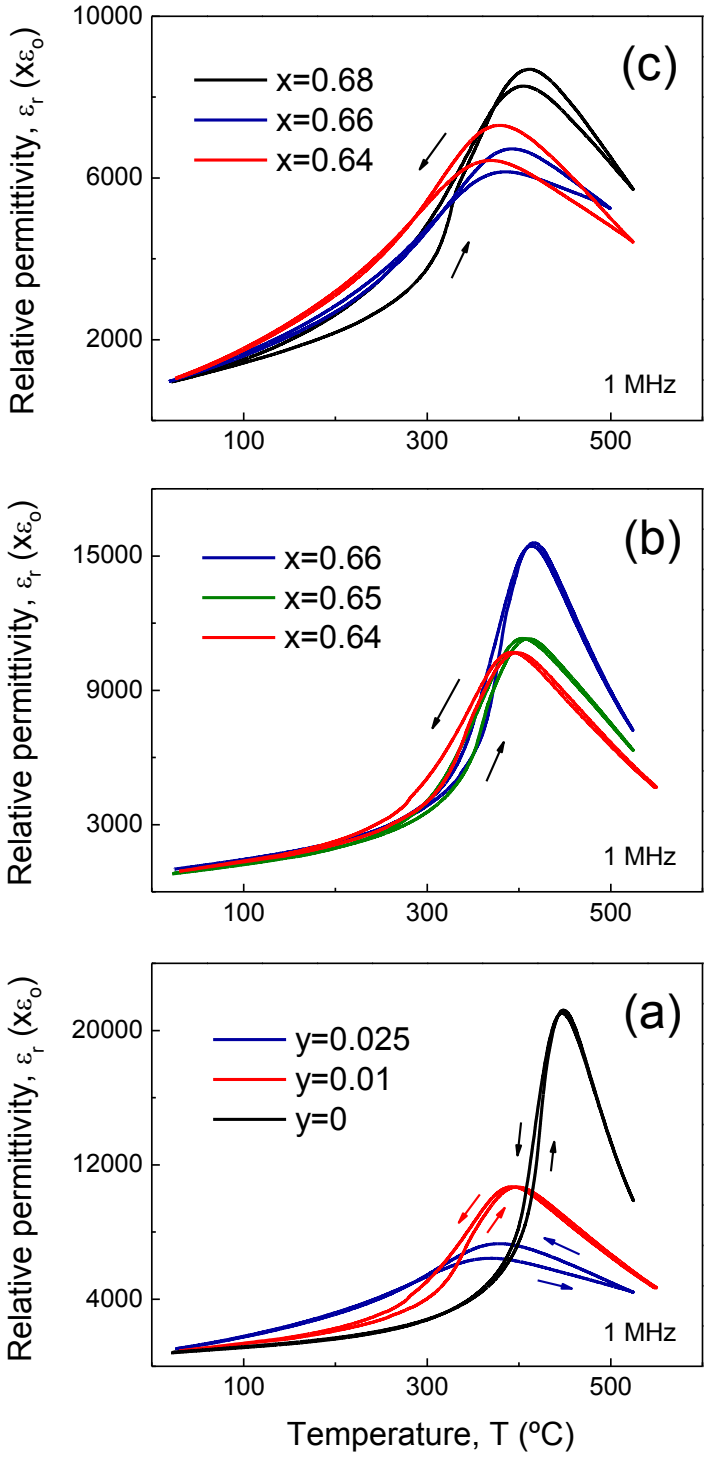

Fig. 6. Temperature dependence of the relative dielectric permittivity of $Bi_{1-x+2y}Pb_{x-3y}Sc_{1-x}Ti_xO_3$ ceramic samples with (a) x=0.64 and y=0, 0.01 and 0.025; (b) x=0.64, 0.65, 0.66 and y=0.01; and (c) x=0.64, 0.66, 0.68 and y=0.025, showing the different evolutions of the ferroelectric transition temperature and dielectric permittivity value with composition.

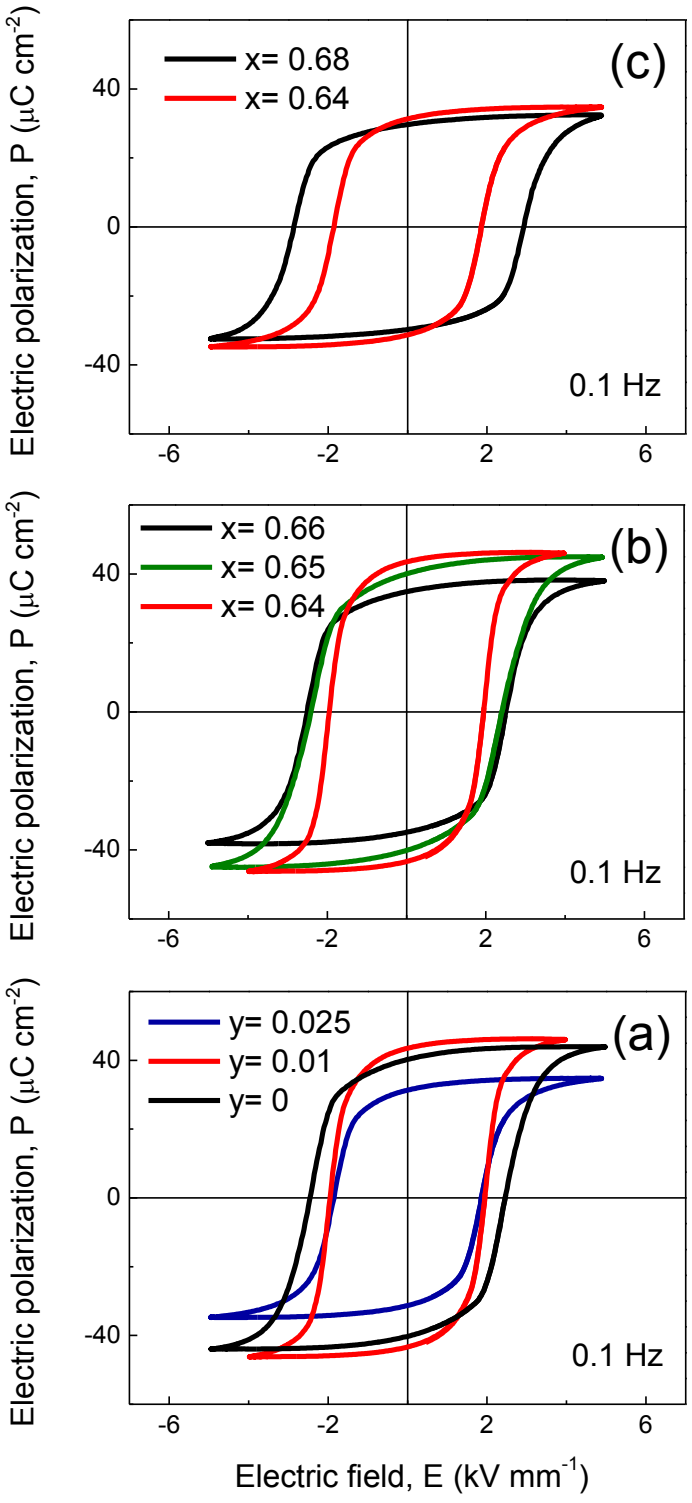

Fig. 7. Ferroelectric hysteresis loops of $Bi_{1-x+2y}Pb_{x-3y}Sc_{1-x}Ti_xO_3$ ceramic samples with (a) x=0.64 and y=0, 0.01 and 0.025; (b) x=0.64, 0.65, 0.66 and y=0.01; and (c) x=0.64, 0.68 and y=0.025, showing the effect of the point defect engineering in the coercitivity and remnant polarization.

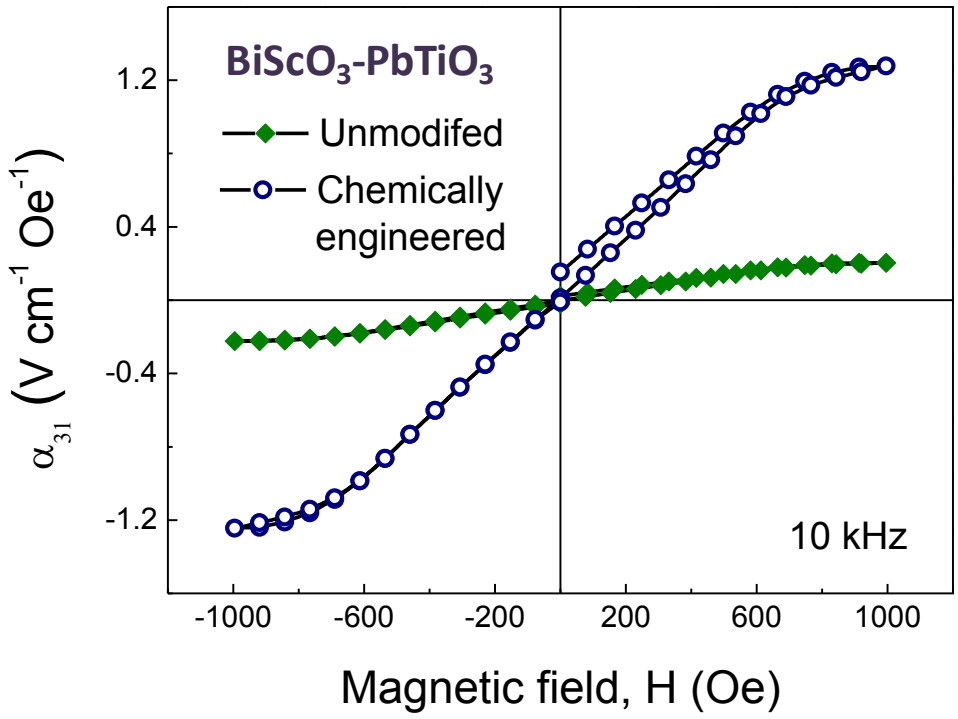

Fig. 8. Magnetoelectric voltage coefficient (α_{31}) as a function of dc magnetic field in L-T mode of three-layer structures fabricated with Terfenol-D and either the unmodified $BiScO_3$-$PbTiO_3$ or the chemically engineered material that incorporates the A-site non-stoichiometry; that is, $Bi_{1-x+2y}Pb_{x-3y}Sc_{1-x}Ti_xO_3$ with x=0.64 and y=0, and with x=0.64 and y=0.01, respectively.